



Fermi National Accelerator Laboratory

FERMILAB-Conf-96/229-E

D0

Upgrade Plans for the D0 Calorimeter

Jonathan Kotcher

Representing the D0 Collaboration

*Fermi National Accelerator Laboratory
P.O. Box 500, Batavia, Illinois 60510*

*Brookhaven National Laboratory
Upton, New York 19973*

August 1996

Submitted to the *6th International Conference on Calorimetry in High Energy Physics*, Laboratori Nazionali di Frascati (INFN), Rome, Italy, June 8-14, 1996

Disclaimer

This report was prepared as an account of work sponsored by an agency of the United States Government. Neither the United States Government nor any agency thereof, nor any of their employees, makes any warranty, expressed or implied, or assumes any legal liability or responsibility for the accuracy, completeness, or usefulness of any information, apparatus, product, or process disclosed, or represents that its use would not infringe privately owned rights. Reference herein to any specific commercial product, process, or service by trade name, trademark, manufacturer, or otherwise, does not necessarily constitute or imply its endorsement, recommendation, or favoring by the United States Government or any agency thereof. The views and opinions of authors expressed herein do not necessarily state or reflect those of the United States Government or any agency thereof.

Distribution

Approved for public release; further dissemination unlimited.

UPGRADE PLANS FOR THE DØ CALORIMETER

Jonathan Kotcher
(representing the DØ Collaboration)
Brookhaven National Laboratory
Upton, New York 11973, USA

ABSTRACT

The DØ detector, a large collider detector located at the Fermi National Accelerator Laboratory, has begun implementing a major detector upgrade in anticipation of the completion of the Main Injector project at the Fermilab Tevatron. The calorimeter readout has been redesigned in order to accommodate the factor of ≈ 10 increase in instantaneous luminosity and the decrease in the inter-bunch separation. Our means of dealing with the increased event rates, along with our plan for controlling overall noise levels in the calorimeter, are discussed. We also present a brief overview of the design for the detector upgrade, including a discussion of some of the more cogent physics topics that will be accessible with the factor of ≈ 20 increase over the present data sample.

1 Introduction

The DØ detector, ¹⁾ located at the Fermi National Accelerator Laboratory in Batavia, Illinois, USA, is a large hermetic detector designed to study high- p_T phenomena in proton-antiproton collisions at $\sqrt{s} = 1.8$ TeV. The centerpiece of the detector is hermetic, uranium/liquid argon sampling calorimetry, designed to provide high resolution energy measurements over the full solid angle. ²⁾

The laboratory is in the process of completing an accelerator (Main Injector) upgrade that will increase the delivered instantaneous luminosity, \mathcal{L}_{inst} , by about a factor of ten (from $\mathcal{L}_{inst} \approx 10^{31}$ to 10^{32} cm⁻²sec⁻¹). The upgraded machine is expected to begin delivering colliding beam in 1999. In order to best exploit the physics opportunities, extensive upgrades of the three major subdetectors – tracking, calorimetry, and muon – are currently underway. ³⁾

| | Run 1 | Run 2 |
|--|----------------------------|--------------------------|
| Status | May, 1992 – Feb, 1996 | ~ end 1999 |
| \mathcal{L}_{inst} ($\text{cm}^{-2}\text{sec}^{-1}$) | $\sim 10^{31}$ | $\sim 10^{32}$ |
| $\int \mathcal{L} dt$ | $\sim 120 \text{ pb}^{-1}$ | $\sim 2 \text{ fb}^{-1}$ |
| Bunch spacing | $3.5 \mu\text{s}$ | 396 (132) ns |
| Center-of-mass energy | 1.8 TeV | 1.8 (2.0) TeV |
| δM_W (MeV) | 170 (~ 100) | 50 |
| δM_{top} (GeV) | 11 | 5 |

Table 1: Overview of the status of the Tevatron and DØ. Representative physics benchmarks – our preliminary errors for the W boson and top quark masses – are shown for both Runs 1 and 2. (Details are in text.)

This paper is segmented into five major subsections. The first section contains a few introductory remarks. In the second section, we present an overview of the collider program at the Tevatron, a few of the physics topics accessible with the upgraded accelerator, and a short description of the overall detector upgrade. Section 3 contains a more detailed description of the internal structure of the calorimeter, including a discussion of the present readout scheme. The current and future accelerator parameters are presented in Section 4, which is followed by a description of our design for the upgrade of the calorimeter electronics. Of fundamental concern is how the noise will be affected by our design changes – this is discussed in Section 4 as well. A brief summary is presented in Section 5.

2 The DØ Upgrade

2.1 Current Status

An overview of the current status of the Fermilab collider program is shown in Table 1. We have recently completed a major collider run (“Run 1”), in which a data sample of $\approx 120 \text{ pb}^{-1}$ was collected. Our current preliminary results for the total error on both the W mass and the top mass are as shown in the table; in parentheses is shown the W mass error we anticipate after the full analysis of the Run 1 data sample is completed. We expect to improve the precision in both of these channels by about a factor of two after the coming upgrade run (“Run 2”). The center-of-mass energy during Run 2 has not been finalized; for completeness, both of the current options are listed. Two bunch structure scenarios are anticipated (see Section 4). We note the factor of ≈ 20 increase over the current data set after Run 2.

The increase in the instantaneous luminosity, the significant decrease in the

bunch spacing, and the overall physics requirements have all motivated a substantial detector upgrade. The last of these subjects is discussed in the following subsection. The change in the accelerator parameters has played a central role in the design of the calorimeter upgrade; we therefore defer a more detailed discussion of this subject to Section 4.

2.2 Run 2 Physics Topics

As mentioned above, the $\approx 1,000$ background-subtracted top candidates we expect to collect should allow us to measure the top mass to ≈ 5 GeV. The large sample will also allow for a measurement of the CKM matrix element $|V_{tb}|$ to $\approx 3\%$. The reconstruction of ≈ 400 single top events should allow a direct measurement of the full width of the top quark (Γ_{top}) to a precision of $\approx 15\%$.

The W and Z asymmetries will be measured to high precision, with the forward/backward asymmetry from Z decays expected to yield a $\approx 0.1\%$ measurement of $\sin^2 \theta_W$. We expect to improve the limits on the anomalous vector boson couplings by approximately an order of magnitude or more. We also anticipate a measurement of the width of the W to ≈ 50 MeV via the measured shape of the transverse mass distribution.

The large b sample will allow detailed studies of $b\bar{s}$ and $b\bar{c}$ final states, as well as enhanced searches for rare decay modes. Studies of CP violation, as statistics permit, will also be pursued.

Monte Carlo studies have shown that the factor of ≈ 20 in the data set will allow us to significantly extend our reach in searches for supersymmetry, with mass limits improving by about a factor of two over our current values. We will also continue to pursue searches for new, non-standard physics processes.

2.3 The Upgraded DØ Detector

The heart of the DØ upgrade consists of a major redesign of the tracking detectors (see Fig. 1). One of the major components will be a 2 Tesla magnetic field provided by a 2.8 m long solenoidal magnet, which will provide momentum measurements of charged particles via their curvature in the field. Precision measurements of primary and secondary vertices will be provided by a silicon vertex detector (SVX), which immediately surrounds the beampipe in the central region. Surrounding the SVX is a multi-layered scintillating fiber tracker (SFT), which will provide tracking information for charged particles in the range $|\eta| < 1.7$.⁴⁾ At the outer radius of the solenoid will be a central preshower (CPS), which will provide energy and position measurements of showering particles, enhancing electron identification over a broad range in p_T . The technology for the CPS consists of triangular scintillator

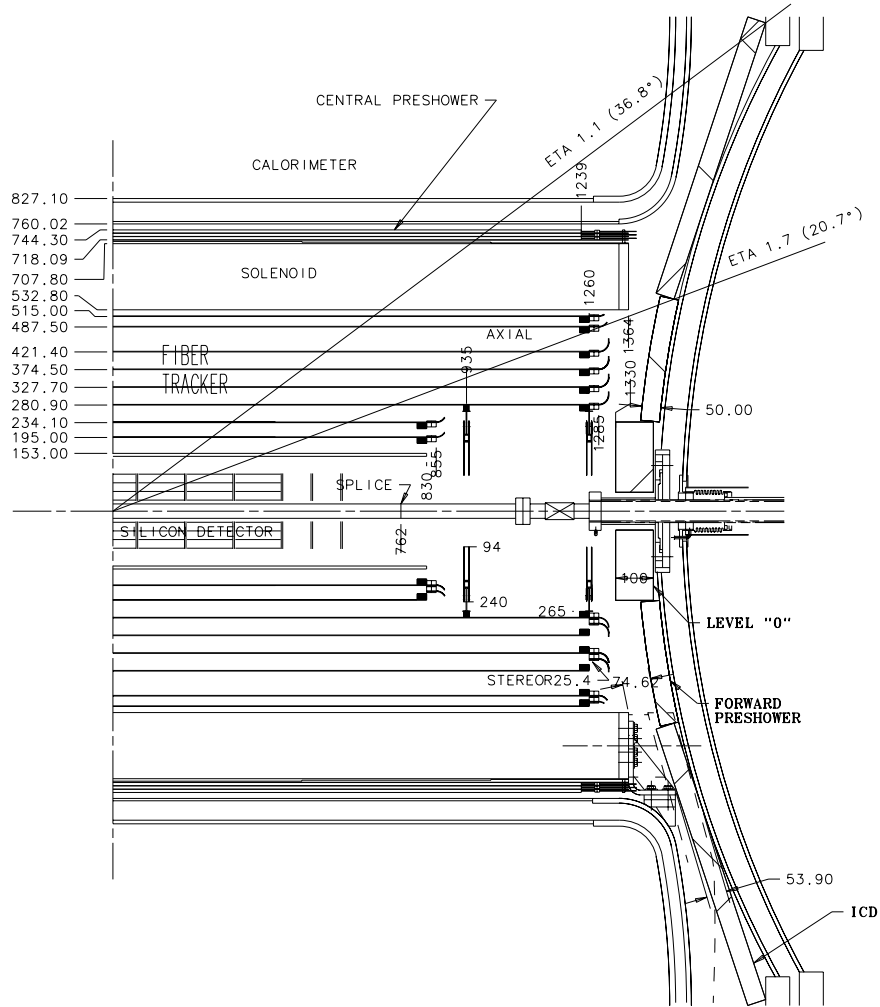


Figure 1: The view in r - z of one half of the central region of the upgraded DØ detector, showing the silicon, scintillating fiber, and preshower detectors, and the magnet solenoid.

strips with embedded wavelength shifting fibers. The speed of the SFT readout, in conjunction with new muon trigger detectors and the central preshower, will allow for fast triggering on single muons and electrons, a critical capability for exploiting the physics in Run 2.

Our design extends this capability to the forward region. A forward preshower, employing the same technology and readout as its central counterpart, will cover the range $1.6 < |\eta| < 2.5$. To complement the tracking in the central region, we have included two layers of silicon disks at more forward pseudorapidities, which extend the tracking coverage to $|\eta| \approx 3$.

Improvements in the muon system include replacing the forward drift

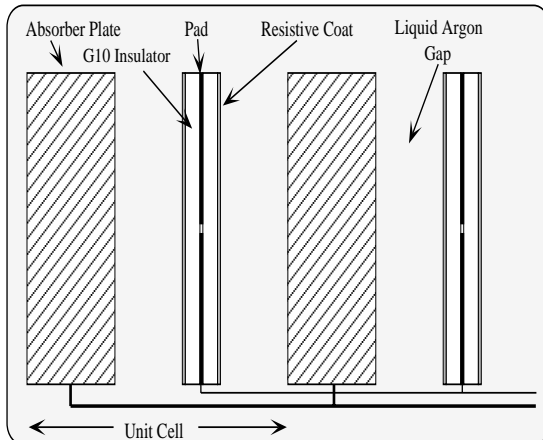


Figure 2: Typical unit cell for the calorimeter, showing the gap structure, the grounded absorber plates, and the signal boards.

chambers with a version that will be more robust in the high-luminosity environment, enhancing the forward shielding to reduce backgrounds, and adding both central and forward scintillator planes to provide fast triggering capability.

3 Calorimeter Structure and Readout

The calorimeter is housed in three cryostats – a central and forward/backward calorimeters, which together cover to $|\eta| \approx 5$ – with the inner volume consisting of a series of structural modules. The readout is arranged into $\approx 5,000$ semi-projective towers of size 0.1×0.1 in $\Delta\eta \times \Delta\phi$, and is segmented longitudinally into electromagnetic (EM), fine hadronic (FH), and coarse hadronic (CH) sections.

Individual calorimeter modules consist of repeating sections of unit cells such as those shown in Fig. 2, which shows a longitudinal section through a typical module. The absorber plates vary in thickness and composition in the different calorimeter regions; the gap spacing between the signal boards and the absorber plates is 2.3 mm throughout. The substrate for the signal boards is composed of G-10, which is coated with a carbon-loaded resistive epoxy to which 2.0 kV high voltage is applied. With the absorber plates at ground potential, this provides the drift field for ionization across the gap. The charge collection time is ≈ 450 ns. In between the two layers of G-10 are etched copper pads, on which signals are capacitively induced by charge drifting across the gap. The G-10 plays the role of a blocking capacitor between the preamplifiers and the high voltage.

The signals are locally ganged (longitudinally) before being directed to the periphery of the modules via multi-layer boards. The details of the ganging depend

on the particular location in the calorimeter. The signals are then sent to the exterior of the calorimeter via 30Ω coaxial cable to preamplifiers housed in boxes atop the cryostats. After amplification and integration, the signals are brought below the detector platform to signal shapers. In addition to performing unipolar shaping, the shapers sample the signal voltage just prior to (the “baseline”) and $2.2\ \mu\text{s}$ after (signal “peak”) the $\bar{p}p$ crossing. The baseline is then subtracted from the peak voltage to obtain the final analog signal.¹ In order to reduce the dynamic range requirements of the digitization that follows, the shaper outputs can be amplified by 1 or by 8, depending on the size of the resulting signal.

Provided a first-level trigger has been fired (see below), the shaper output is multiplexed to analog-to-digital converters (ADC’s) that have 12-bit resolution and 15-bit dynamic range. Upon receiving an appropriate signal from the software trigger, the data is then shipped to a host computer to be recorded. There are a total of 47,800 readout channels for all three cryostats.

In order to equalize the gains for all of the electronics channels (making them independent of cell capacitance), DØ employs a precision calibration pulser that injects charge directly at each preamplifier input. The pulser also monitors, and permits a correction for, any time dependence in the response of the electronics chain to charge in the system.

3.1 Relevant Accelerator Parameters

The bunch structure for Runs 1 and 2 is shown in Fig. 3. The accelerator currently delivers 6 bunches each of protons and antiprotons (“ 6×6 ” bunches), separated by a $3.50\ \mu\text{s}$ gap. This gap is used to form the trigger and sample the detector baselines prior to the next crossing. The formation of this “Level 1” hardware trigger, and the subsequent transport of the signal, takes $\approx 3.0\ \mu\text{s}$, with a majority of this time ($\approx 2\ \mu\text{s}$) being due to intrinsic delays in the cable that route the signals between the front end crates and the trigger framework where the decision is made.

In Run 2, the proton/antiproton bunches circulate in superbunches of $4.36\ \mu\text{s}$ duration, with a $2.64\ \mu\text{s}$ gap spacing between them. The laboratory expects to begin the run with a bunch spacing of 396 ns, evolving to 132 ns as the run progresses. (There will be an additional $\times 3$ more bunches per superbunch here, resulting in 108×108 rather than 36×36). This helps to reduce the number of interactions per bunch crossing, which becomes increasingly important as higher luminosities are achieved. We have been asked to design for this more restrictive 132 ns bunch spacing.

The present electronics has been designed to handle comfortably the 3.50

¹The shapers are commonly referred to as Base-Line Subtractors, or BLS.

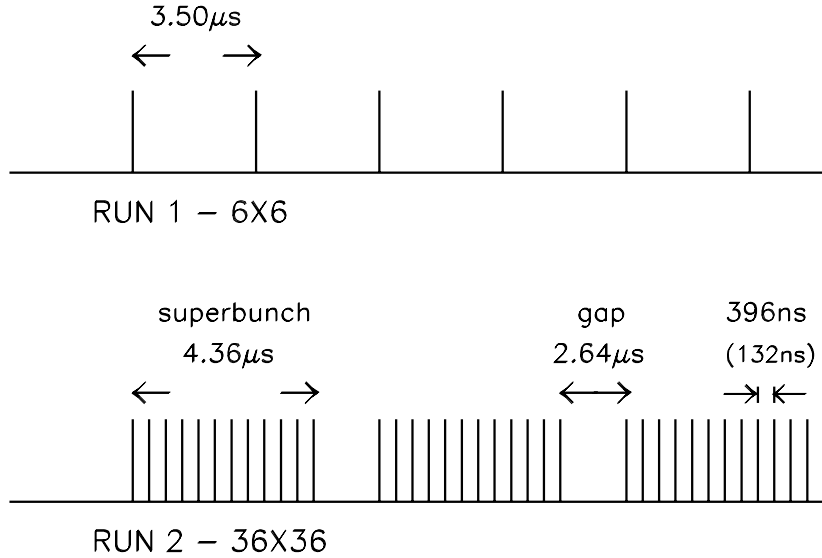


Figure 3: Tevatron bunch scheme for Runs 1 and 2. Details are described in the text. (*Diagram not to scale.*)

μs inter-bunch spacing that was delivered in Run 1: the present $2.2\mu\text{s}$ shaping time and $3.0\mu\text{s}$ trigger-formation time were established with these parameters in mind. The evolution to bunch spacing times that are shorter by an order of magnitude (or more), coupled with the increase in luminosity, dictate that major changes have to be implemented. Of most significance with regard to the calorimeter upgrade is that the calorimeters are welded shut and will not be changed internally. This means that all of the burden for adjusting to the change in accelerator parameters rests solely on the calorimeter electronics, which are external to the calorimeter cryostats.

4 Calorimeter Electronics Upgrade

There are two fundamental considerations that have driven the design of the upgrade electronics:

1. Pileup noise increases with the increase in instantaneous luminosity like $\sim \sqrt{\mathcal{L}_{inst}}$. Shorter shaping times are required to reduce these effects.
2. The reduction in the minimum bunch spacing implies that some type of delay is needed to pipeline the signal.

In order to accommodate item (1), we have gone from the present $2.2\mu\text{s}$ shaping time to 400ns . The increase in electronics noise that is associated with this decrease in the shaping time has motivated our decision to replace all 50,000 preamplifiers with a dual FET version (see Section 4.2). A low noise driver stage

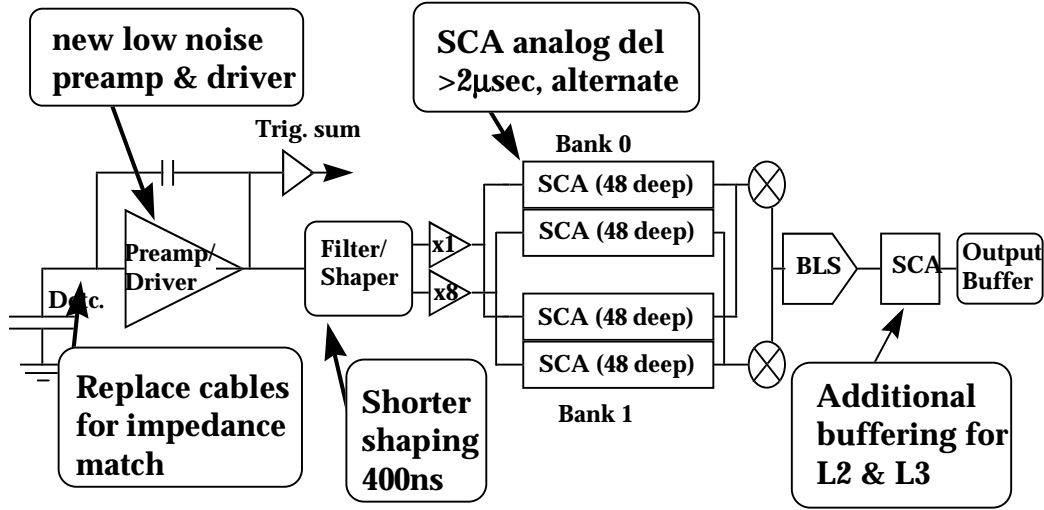


Figure 4: Schematic diagram of the calorimeter upgrade electronics.

is also being included in the preamplifier design. In response to item (2), we have opted to implement Switched Capacitor Arrays (SCA's). These are 48-element-deep analog storage devices that have been designed to provide the necessary amount of buffering capability at 132 ns crossing times. The system has been designed so that the present ADC's can be used: hence, the dynamic range and resolution of the digital readout will remain the same. A block diagram of the calorimeter electronics upgrade is shown in Fig. 4.

The $\times 1$ and $\times 8$ outputs for each channel are stored in an independent SCA element. There are two SCA banks per channel, allowing one to remain “alive” for data storage in the current crossing while the other is read out, helping to minimize dead time. An additional SCA, located just after the baseline subtraction, is used to store the data while awaiting a higher-level (“Levels 2 and 3”) trigger decision. We estimate that, with the dual-bank design, there will be little or no dead time at Level 1 trigger rates up to ≈ 10 kHz, which is the maximum Level 1 rate we are designing for. (This assumes one trigger per superbunch). The system has also been designed to read out multiple triggers within a superbunch; this, however, is expected to result in a small but finite amount of dead time. The output SCA is used as a 48-deep buffer employed to help smooth out rate fluctuations.

4.1 Other Modifications

Both items (1) and (2) demand that significant infrastructure modifications be implemented as well. Approximately 1,200 110Ω cables from the cryostat feedthroughs

to the preamplifier inputs have been replaced with impedance-matched 30Ω cables to minimize sensitivity to reflections. A new version of the preamplifier motherboards is being designed, in which pulser trace capacitances will be reduced and power feeds rearranged. The BLS motherboards will be redesigned to accommodate new pinouts for SCA controls. In addition, a new timing control system, which coordinates signals routed between the ADC and BLS crates, is being designed. A new pulser calibration system and design, which address the constraints that shorter shaping times introduce, will also be needed for relative channel-to-channel calibration and electronics gain monitoring.

4.2 Noise Considerations

We have designed the upgrade electronics to provide the same noise performance as the current readout. The electronics noise increases with shorter shaping times t as \sqrt{t} , but is reduced by about a factor of $\sqrt{N_{FET}}$, or $\sqrt{2}$, through the introduction of the dual FET preamplifier. Uranium noise decreases, again by $\sim \sqrt{t}$, due to the shorter shaping times. As already mentioned, pileup noise increases by a factor $\sim \sqrt{\mathcal{L}_{inst}}$ due to the increase in luminosity, but decreases with the shaping time by $\sim \sqrt{t}$. As a benchmark, our current per-channel electronics noise – the *rms* width of the noise measured *in situ* that is due to electronics sources alone ($\langle \sigma_{el} \rangle$) – is ≈ 5 (30) MeV for the electromagnetic (hadronic) section. The *rms* width of the pedestal distribution ($\langle \sigma_{ped} \rangle$), which represents the contributions from uranium and electronics noise added in quadrature, is ≈ 10 (70) MeV for each of the sections, respectively.

Using the above relations, one can compare the noise performance of the current electronics to that expected after the calorimeter electronics upgrade. In Run 2, the electronics (pileup) noise will increase by approximately a factor of 1.6 (1.3), and the uranium noise will decrease by a factor of ≈ 2.3 . The product of these factors is about equal to unity, implying that the overall noise performance with the new electronics at $\mathcal{L}_{inst} = 10^{32} \text{ cm}^{-2}\text{sec}^{-1}$ will be comparable to that with the old electronics at $\mathcal{L}_{inst} = 10^{31}$. A detailed simulation⁵⁾ of the pileup contribution to a benchmark measurement – the mass of the W boson – has indicated that, relative to our current W mass measurement, no additional mass or resolution bias can be expected at the higher design luminosities with the new electronics.

4.3 Status

We have developed three SCA prototypes, all of which have performed as designed. Cell-to-cell variations have been measured to be less than 0.5 mV, or ≈ 0.5 ADC counts in our unit of readout. Ten-wafer production has recently begun, which will

result in the fabrication of $\approx 1,000$ devices. We are planning a test of a “quadrant” of electronics, which corresponds to 1/12 of the total number of channels or one preamplifier box, including the final SCA chip, this fall.

Other modifications, which include the cable replacements, BLS and preamp motherboard redesign, and preamplifier and shaper fabrication, are on track for a 1999 start date.

5 Conclusions

The upgraded DØ detector has been optimized for the physics of interest in the Main Injector era. Introduction of the silicon vertex and scintillating fiber systems, a central magnetic field, the homogeneous preshower system, and significant muon upgrades will all contribute to the accessibility of a broad range of physics at the upgraded Tevatron.

The calorimeter upgrade has been designed to respond to the challenges introduced by the increased luminosity and the change in accelerator bunch structure, enabling us to maintain the high calorimetric performance we have achieved during Run 1. The design appropriately addresses our need for data storage in the high rate environment, and controlling any associated increases in noise from the three major sources.

References

1. DØ Collaboration, S. Abachi *et al.*, *Nucl. Instr. Meth.* **A338**, 185 (1994).
2. J. Kotcher, “Design, Performance, and Upgrade of the DØ Calorimeter”, *Proceedings of the 1994 Beijing Calorimetry Symposium*, IHEP - Chinese Academy of Sciences, Beijing, China, October 25-27, 1994, pp. 144-158; J. Kotcher, “Physics with the DØ Calorimeter”, these proceedings.
3. DØ Collaboration, “The DØ Upgrade”, DØ Internal Note # 2542 (April 17, 1995).
4. The pseudorapidity, η , is defined by the relation $\eta \equiv -\ln[\tan(\theta/2)]$, where θ is the polar angle with respect to the proton-beam direction. The z axis in the DØ coordinate system is along the beam axis, r is the distance perpendicular to that axis, and ϕ is the polar angle.
5. P. Nemethy and A. Mincer, “Pileup Effects on W Mass Measurement”, DØ Internal Note # 1398 (April, 1992).